ADVANCED FUNCTIONAL MATERIALS

FULL PAPER

DOI: 10.1002/adfm.200600494

New Organic Nonlinear Optical Polyene Crystals and Their Unusual Phase Transitions**

By *O-Pil Kwon*,* *Seong-Ji Kwon*, *Mojca Jazbinsek*, *Ashutosh Choubey*, *Volker Gramlich*, and *Peter Günter*

A series of new nonlinear optical chromophores based on configurationally locked polyenes (CLPs) with chiral pyrrolidine donors are synthesized. All CLP derivatives exhibit high thermal stability with decomposition temperatures T_d at least > 270 °C. Acentric single crystals of enantiopure D- and L-prolinol-based chromophores with a monoclinic space group $P2_1$ exhibit a macroscopic second-order nonlinearity that is twice as large than that of analogous dimethylamino-based crystal. This is attributed to a strong hydrogen-bonded polar polymer-like chain built by these molecules, which is aligned along the polar crystallographic *b*-axis. Five α-phase CLP crystals with different donors grown from solution exhibit a reversible or irreversible thermally induced structural phase transition to a β-phase. These phase transitions are unusual, changing the crystal symmetry from higher to lower at increasing temperatures, for example, from centrosymmetric to non-centrosymmetric, enhancing their macroscopic second-order nonlinear optical properties.

1. Introduction

Organic nonlinear optical materials are of a great interest for photonic applications like microring filters and modulators[1] because of their high and fast nonlinearities and a wide variety of design possibilities.[2] A major challenge for second-order nonlinear optical organic crystals is to simultaneously achieve large macroscopic nonlinearities by spontaneous acentric packing of highly nonlinear optical molecules and thermal/chemical stability of the molecules to apply appropriate crystal-growth-engineering techniques. Numerous molecular engineering investigation have already resulted in very large microscopic molecular nonlinearities of the nonlinear optical chromophores.[3–6] However, in most cases, highly nonlinear optical molecules tend to pack in a centrosymmetric or non-optimal arrangement in the crystalline solid state because of their large dipole moment. Moreover, their thermal stabilities are often not sufficient to apply melt-based crystal growth techniques, which are more attractive because of faster growth rates and generally better crystalline quality without solvent or solution inclusion problems associated with conventional solution growth. In order to achieve a macroscopic second-order nonlinearity, many different approaches have been investigated including the introduction of molecular asymmetry, chirality, steric substituents, hydrogen bonds, Coulomb interaction into chromophores,[2,3,7] supramolecular synthetic co-crystals,[8] and octupolar compounds.[9,10] The most well-known example of an ionic crystal using Coulomb forces to bind molecules is 4′-dimethylamino-*N*-methyl-4-stilbazolium tosylate (DAST), which exhibits a large macroscopic second-order nonlinearity about 1000 times larger than that of urea at 1.9 μm,[11,12] but shows insufficient thermal stability for melt growth. Other investigations have been focused on improving the thermal stability of chromophores.[13–15] However, there are only a few reports on the successful development of simultaneously highly nonlinear optical crystals and reliable thermal stability for melt-based crystal growth techniques.

Recently we demonstrated organic nonlinear optical single-crystalline thin films by melt growth techniques.[16] The configurationally locked polyene (CLP) chromophore used for the growth, 2-{3-[2-(4-dimethylaminophenyl)vinyl]-5,5-dimethylcyclohex-2-enylidene} malononitrile (DAT2), exhibits a large macroscopic nonlinearity with two orders of magnitude greater powder second harmonic generation (SHG) intensity than that of urea at 1.9 μm and high thermal stability with a decomposition temperature T_d of over 290 °C. However, the effect of structural modifications of the CLP chromophore on the crystal structure has not yet been fully studied.

We report herein a series of new nonlinear optical chromophores based on CLPs with a chiral pyrrolidine electron donor in order to improve the non-centrosymmetric packing of chromophores into a crystal structure, while still keeping the high thermal stability of the CLP chromophores for melt-based crystal growth engineering. Acentric single crystals of enantiopure D- and L-prolinol-based chromophores with monoclinic space group $P2_1$ exhibit two times larger macroscopic nonline-

[*] Dr. O-P. Kwon, S.-J. Kwon, Dr. M. Jazbinsek, Dr. A. Choubey, Prof. P. Günter
Nonlinear Optics Laboratory, ETH Zurich
8093 Zurich (Switzerland)
E-mail: kwon@phys.ethz.ch
Prof. V. Gramlich
Laboratory of Crystallography, ETH Zurich
8093 Zurich (Switzerland)

[**] This work has been supported by the Swiss National Science Foundation.

ADVANCED FUNCTIONAL MATERIALS

arity than the analogous DAT2 crystal. Five α-phase CLP crystals grown from solution exhibit a thermally induced phase transition to a β-phase. Their phase transition from a low-temperature higher symmetry crystalline structure to a high-temperature lower symmetry structure, which is either reversible or irreversible, is rather unusual, and to our knowledge, observed for the first time in organic nonlinear optical crystals with large molecular dipole moment. Therefore, the β-phase crystals can exhibit even larger macroscopic second-order nonlinearities than the α-phase.

2. Results and Discussion

2.1. Synthesis and Characterization

The chemical structures of the newly synthesized chromophores are shown in Figure 1. The chromophores consist of the configurationally locked π-conjugated phenylhexatriene bridge linked between a pyrrolidine (Py) electron donor and a dicyanomethylidene [>C=C(CN)$_2$] electron acceptor. The non-π-conjugated part in the hexatriene bridge is connected with equatorial and axial methyl groups (PyT series) or hydrogen atoms (PyM series). Six of the investigated chromophores incorporate the chiral hydroxyl (OH) group to induce strong hydrogen bonding in the crystalline state. The chromophores were synthesized by consecutive Knoevenagel condensations according to literature procedures.[15–17] To introduce the chirality of the hydroxyl group on the pyrrolidine ring the enantiopure pyrrolidine derivatives such as D-3-pyrrolidinol (98 %), D-prolinol (99 %), and L-prolinol (99 %) were used for the synthesis. After the synthesis, the material used for all the experiments was purified by recrystallization from methylenechloride/methanol several times.

The results of physical and structural measurements including the phase transition, melting and decomposition temperature, the wavelength of maximum absorption, and crystalline space groups are summarized in Table 1. The wavelength of maximum absorption λ_{max} for the newly synthesized CLP chromophores is in the range of 503–521 nm in chloroform solution. The values of maximum absorption λ_{max} are similar as for the DAT2 chromophore, having high molecular nonlinearity ($\beta_z = 1100 \times 10^{-40}$ m^4 V^{-1} determined by electric-field induced second harmonic generation measurements at the wavelength of 1907 nm).[16] This is because λ_{max} is related to the π-conjugated part, including the donor and acceptor groups, according to the so-called nonlinearity–transparency tradeoff.[2,16] This indicates that the structural modifications of the non-π-conjugated part of the newly synthesized chromophores do not affect the high microscopic molecular nonlinearity of DAT2-analogous chromophores but only lead to different crystalline packing and macroscopic nonlinearity.

The thermal stabilities of the CLP chromophores were investigated by thermogravimetric analysis (TGA) and differential scanning calorimetry (DSC) under a nitrogen atmosphere at a scan rate of 10 °C min^{-1}. The melting temperature T_m is defined here as the end point of the endothermic transition in the DSC scan. The decomposition temperature T_d was estimated as the temperature at the intercept of the leading edge of the weight loss, that can involve sublimation and/or decomposition, by the base line of the TGA scans. The results of these measurements are given in Table 1. All CLP chromophores exhibit a very high T_d at least > 270 °C and moreover exhibit large temperature differences between the T_d and T_m. The thermal properties are therefore advantageous for applying melt-based crystal growth engineering.

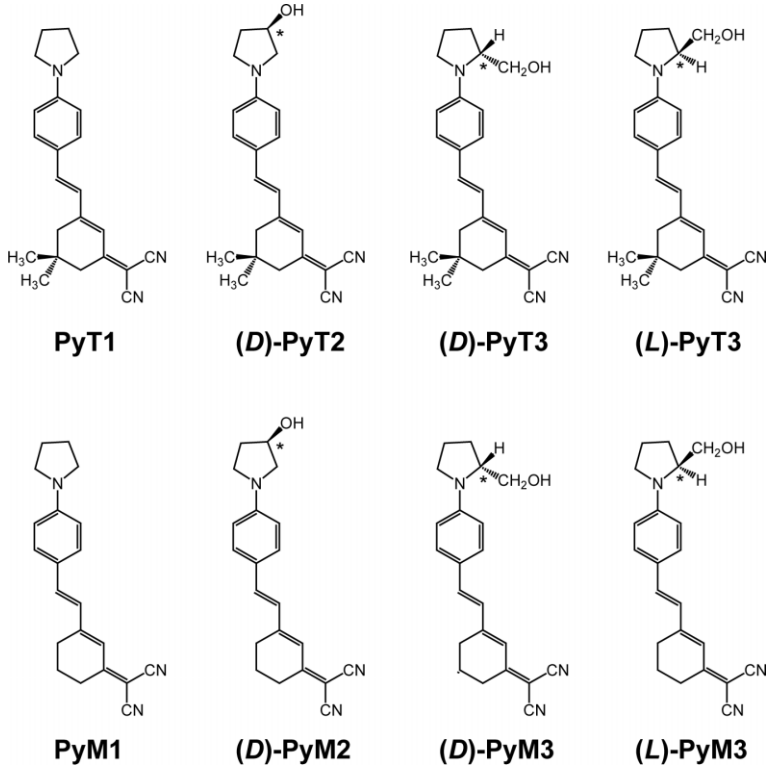

Figure 1. The chemical structures of the investigated configurationally locked polyene chromophores with pyrrolidine donor.

2.2. Macroscopic Nonlinearities and Single-Crystal Structures

Single crystals were grown from methylenechloride/methanol (ca. 1:2) solution by the slow-evaporation method. We define here the phase of the crystal as grown from the solution as α-phase and the phase of the crystal after the phase transition as β-phase, which is presented later on. For screening the macroscopic nonlinearity of the new CLP crystals the Kurtz and Perry powder test[18] was performed at a fundamental wavelength of 1.9 μm using an optical parametric amplifier pumped by an amplified Ti:sapphire laser. We compared the second harmonic generation (SHG) signal with the DAT2 crystalline powder, which possesses a strong second harmonic activity of

Table 1. Results of physical and structural measurements of the CLP crystals. Powder second harmonic generation measured at a fundamental wavelength of 1.9 μm relative to that of DAT2 powder (about two orders of magnitude larger than urea) from Ref. [16]. λ_{max}: the wavelength of the maximum absorption in chloroform solution, T_d: the decomposition temperature determined by thermogravimetric analysis (TGA), T_{tr}: the phase transition temperature, T_m: the melting temperature determined by differential scanning calorimetry (DSC).

	λ_{max} [nm]	T_{tr} [°C]	T_m [°C]	T_d [°C]	Space group [a]	Powder SHG	
						α-phase [a]	β-phase [b]
PyT1	521	85 ± 3	178	290	$P2_1$	0.6	1.0
PyT2	510	N [c]	191	288	–	0	–
(D)-PyT3 (L)-PyT3	506	180 ± 5	211	300	–	0	0.9
PyM1	518	N [c]	257	275	–	0	–
PyM2	506	N [c]	200	288	–	0	–
(D)-PyM3 (L)-PyM3	503	160 ± 5	213	270	$P2_1$	2.0	2.0
DAT2	502	N [c]	235	293	$P2_1$	1.0	–

[a] Before and [b] after the phase transition. [c] N means that the α-phase crystal grown from solution did not exhibit a phase transition before melting.

about two orders of magnitude larger than that of urea.[16] Three α-phase crystalline powders grown from the solution exhibited strong second harmonic generation activities of 0.6, 2.0, and 2.0 times that of DAT2, that is, PyT1, D-PyM3, L-PyM3, respectively (see Table 1).

In order to check if enantiopure D- and L-polyene crystals with chiral hydroxyl groups have different crystal structures, powder X-ray diffraction patterns were measured. The D- and L-PyM3 crystals grown by the above-mentioned slow-evaporation method show equivalent powder X-ray diffraction patterns, as shown in Figure 2a, even though they exhibit different morphologies of needles and/or triangular plates. The centrosymmetric enantiopure D- and L-PyT3 crystals also show equivalent powder X-ray diffraction patterns (see Fig. 2b). Note that the enantiopure D- and L-polyene crystals in our work exhibit an identical crystal structure without polymorphism, but with different absolute configurations such as (D)* and (L)* crystals[19] that possess opposite handedness (if in one orientation of the constituent molecule is fixed to the crystallographic +*b*-axis, in the other it is fixed to the –*b*-axis). The details of the different morphology in the enantiopure crystals due to different growth conditions will be discussed elsewhere.

Single-crystal structure for the acentric α-phase CLP crystals were determined by X-ray diffraction and are given in Table 1. The PyT1 and PyM3 crystals have non-centrosymmetric structures, all monoclinic with space group symmetry $P2_1$ (point group 2). Because of its highest macroscopic nonlinearity, we discuss the PyM3 crystallographic structure in more detail in this paper. Figure 3 shows the molecular structure of the L-PyM3 as determined by single crystal X-ray analysis. The pyrrolidine ring is arranged in the so-called half-chair configuration as reported previously for *N*-(4-nitrophenyl)-L-prolinol (NPP) crystal.[20] The main part of the π-conjugated bridge from the nitrogen atom (N) of the pyrrolidine donor group to

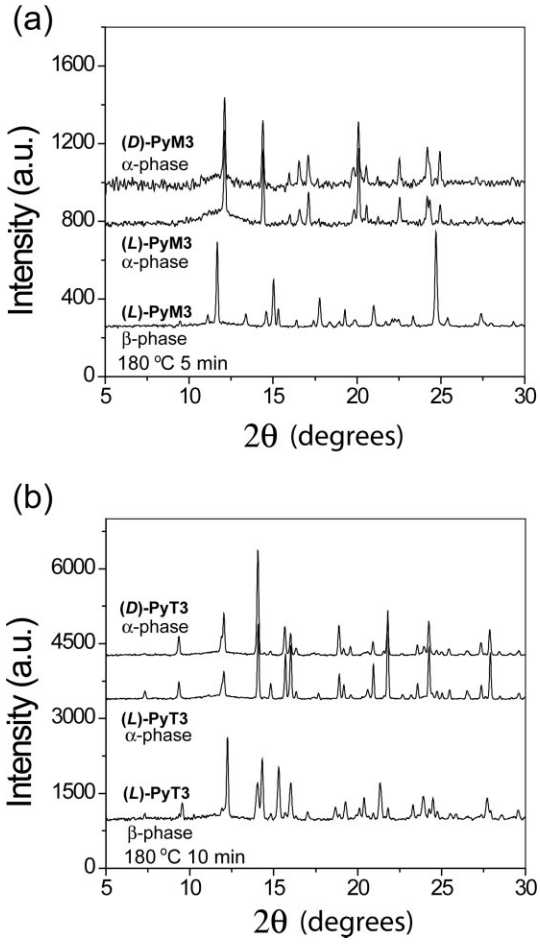

Figure 2. Powder X-ray diffraction patterns of a) PyM3 and b) PyT3 crystals: from top to bottom, enantiopure D- and L-α-phase crystalline powders, L-β-phase crystalline powder, which is prepared by isothermal heat treatment at 180 °C.

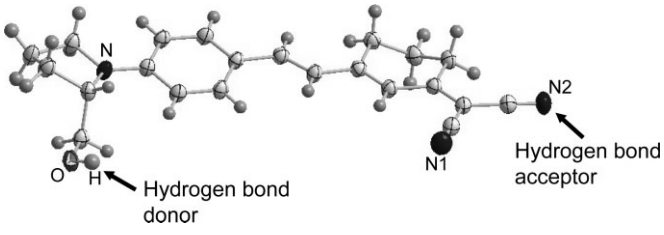

Figure 3. Molecular structure of the L-PyM3 chromophore as determined by X-ray crystallography in the α-phase crystalline state.

the nitrogen atom (N2) of one of the cyano acceptor groups is nearly planar (twist angle ca. 1°). The phenyl ring and the cyano groups corresponding to the nitrogen atom (N1) are slightly out of plane from the main π-conjugated bridge (twist angle ca. 6°). A nearly planar π-conjugated bridge is important for an efficient π-electron delocalization and thus ensures a large molecular nonlinearity in the crystalline solid. Another interesting aspect of the PyM3 molecule is that there are two hydrogen-bonding sites, as shown in Figure 3. One site corre-

ADVANCED FUNCTIONAL MATERIALS

sponds to the nitrogen atom (N2) on the electron acceptor group that acts as the hydrogen bond acceptor. The other site corresponds to the hydrogen atom on the OH group in the pyrrolidine ring that acts as the hydrogen bond donor. As shown in Figure 4, the L-PyM3 crystal exhibits a non-centrosymmetric packing of the chromophores, monoclinic with space group symmetry $P2_1$ (point group 2). The nitrogen atom (N2) on the CN group and the hydrogen atom on the OH group are linked by a strong hydrogen bond with a H···N distance of about 2.04 Å. With the help of these two hydrogen bonding sites at opposite ends, L-PyM3 molecules build a hydrogen-bonded polar polymer-like chain in the crystalline solid (see Fig. 4a). Another striking feature of the packing is that the polar polymer-like chains are stacked up one by one and are perfectly aligned along the principal crystallographic polar *b*-axis, as shown in Figure 4b. In the case of the analogous DAT2 crystal that does not contain the hydroxyl (OH) group, the DAT2 molecules are also aligned along the principal crystallographic polar *b*-axis, but in a mutually crossed fashion without interlayer stacking (see Fig. 5a). The macroscopic second-order nonlinear optical response d_{333} is roughly estimated by $d_{333} = N\beta f(\omega) <\cos^3\theta_p>$, where N is number of molecules per unit volume, $f(\omega)$ the local field factor, and θ_p the angle between the molecular-charge-transfer axis and the polar crystalline axis.[2] The reason for the larger macroscopic nonlinearity of the L-PyM3 crystal in the powder SHG test as compared to the analogous DAT2 crystal can be related to the order parameter $\cos\theta_p$. As shown in Figure 5b, the long axis of the L-PyM3 molecule, which is a favorable direction of charge delocalization, is more aligned along the crystallographic polar *b*-axis than for DAT2.

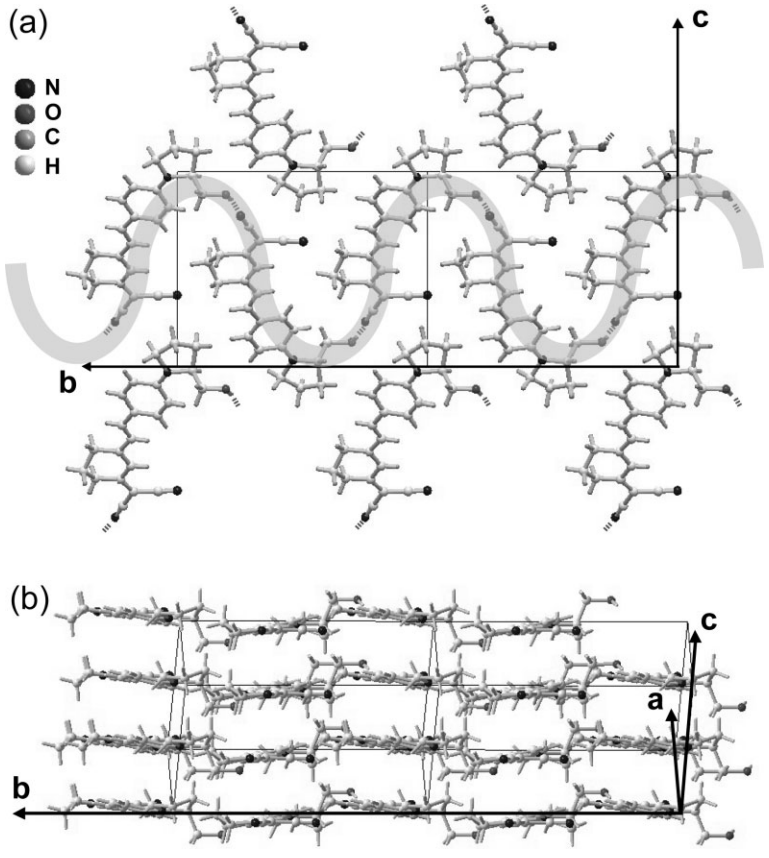

Figure 4. Crystal packing diagram of L-PyM3 chromophore of the monoclinic $P2_1$ crystal structure (α-phase) a) projected along the *a*-axis and b) side view of a stack of acentric layers aggregated by hydrogen-bonded chains. Molecules in a chain are linked with hydrogen bonds, which are indicated by dashed lines.

2.3. Thermally Induced Phase Transitions

In the DSC measurements, the five CLP crystals grown from the solution of PyT1, D-PyM3, L-PyM3, D-PyT3, and L-PyT3 exhibit a phase transition from an α-phase to a β-phase as shown in Figures 6 and 7. All the heat flows corresponding to a phase transition before the melting occur very far from the decomposition temperatures T_d. Therefore, the observed transitions are not related to any decomposition process. In the case of very polar organic materials, one would expect that the transformation processes with increasing temperature are from a lower symmetry to a higher symmetry arrangement, for example, from a polar to a nonpolar structure, because of the tendency for dipole–dipole aggregation of chromophores with a large dipole moment. However, as we show in the following, the phase transitions of the CLP crystals, either reversible or irreversible, are unusual, changing the crystal symmetry from a higher to a lower one when the temperature is increased.

In the case of PyT1 crystals without the OH group, a reversible endothermic structural phase transition occurs at $T_{tr} = 85 \pm 3$ °C upon heating and an exothermic transition at 66 ±3 °C upon cooling, as shown in Figure 6a. Both transitions are well below the melting temperature of $T_m = 178$ °C. Polymorphs obtained by the phase transition can be classified as either enantiotropic or monotropic, depending on whether the transition is reversible or irreversible, respectively.[21,22] The observed phase transition of PyT1 crystals is reversible enantiotropic, with one polymorphic form that is thermodynamically stable below the transition temperature and the other above the transition temperature.[21,22] The transitions are reversible, as has been shown by an isothermal heat treatment at 120 °C for 20 min. Cooling to room temperature results in an identical α-phase crystal structure as before the heat treatment and phase change. Therefore the transformation of PyT1 crystals is fully reversible. The β-phase PyT1 crystalline powder at 100 °C exhibits an SHG efficiency 1.7 times larger than in the α-phase. Therefore, we can conclude that the phase transition of the PyT1 crystals from the α-phase to the β-phase is a structural transition from one non-centrosymmetric phase to a different non-centrosymmetric phase.

The prolinol-based CLP crystals containing the chiral OH group, D-PyM3, L-PyM3, D-PyT3, and L-PyT3, also exhibit a phase transition. In contrast to the reversible phase transition of the PyT1 crystal with a small endothermic peak, the characteristics of the transition for prolinol-based CLP crystals in the

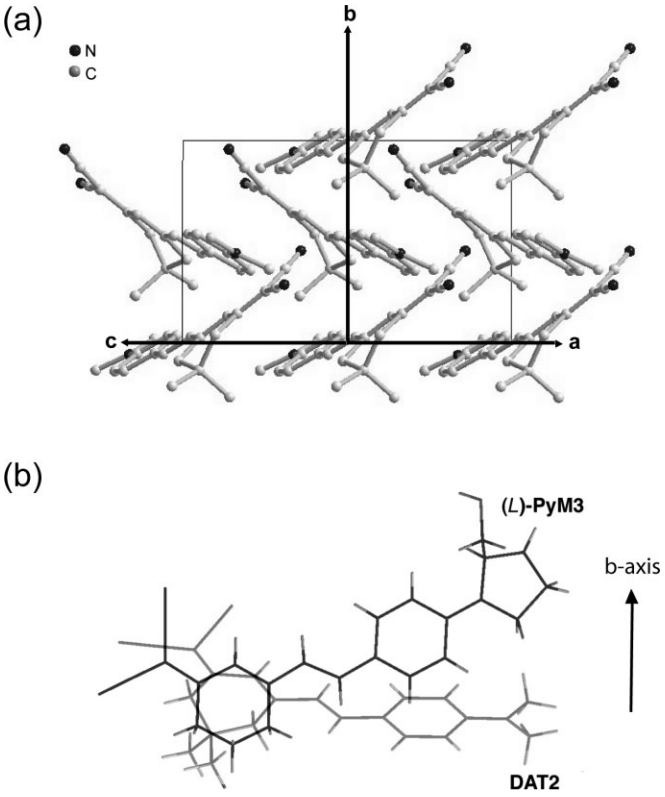

Figure 5. a) Crystal packing diagram of DAT2 chromophore of the monoclinic $P2_1$ crystal structure. The H atoms are omitted. b) Two superimposed molecules of L-PyM3 and DAT2 to point out the difference in crystalline packing.

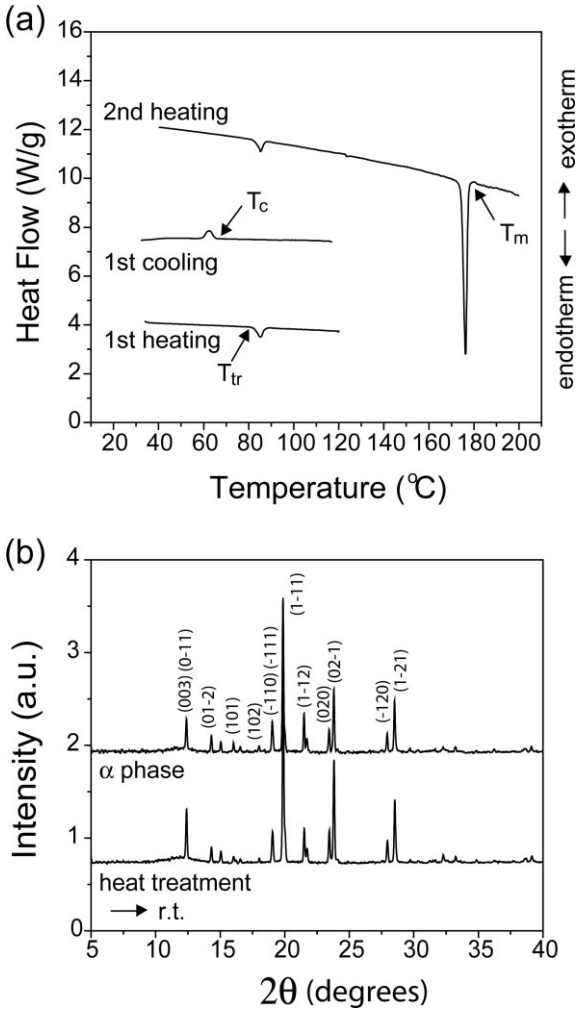

Figure 6. Reversible phase transition of red platelike PyT1 crystals: a) DSC thermograms (10 K min^{-1} scan rate) and b) powder X-ray diffraction patterns: α-phase crystalline powder (top), crystalline powder after an isothermal heat treatment at 120 °C for 20 min and cooling down to room temperature(bottom). Note that the two X-ray diffraction patterns show equivalent crystalline properties indicating that the phase transition is reversible.

DSC measurements are dependent on the crystal morphology (see Fig. 7); for example, for L-PyM3 crystals, one small endothermic peak for a needlelike morphology is observed or two large peaks (endothermic melting and exothermic recrystallization) for a crystalline powder mixture, all below the melting transition (see Fig. 7). The reason for the dependence of the transition characteristics on the morphology might be linked to kinetic and steric hindrance of the solid–solid transition of long rod-shaped chromophores.[21,22]

The other different characteristic of the phase transitions in the prolinol-based CLP crystals as compared to the PyT1 crystals is that the transition is irreversible, as shown in the DSC curves represented in Figure 8. In order to investigate the changes of the molecular arrangements by the phase transitions we measured powder X-ray diffraction patterns as well as IR absorption spectra. The β-phase of PyM3 and PyT3 crystals, obtained by isothermal heat treatment at 180 °C for 5 min and 10 min, respectively, exhibit different crystallographic structures as confirmed by powder X-ray diffraction measurement performed after the heat treatment, as shown in Figure 2. In the IR spectra, the O–H stretching absorptions of the hydroxyl groups are related to intermolecular hydrogen bonding. In general, the stretching vibrations of "free" and intermolecularly hydrogen-bonded hydroxyl groups give a sharp peak in the 3590–3650 cm^{-1} region and a broad peak in the 3200–3550 cm^{-1} region, respectively. In both PyM3 and PyT3 crystals the O–H stretching absorption peaks of the β-phase crystals are shifted towards higher wavenumber (i.e., closer to "free" hydroxyl groups) than that of the α-phase: 3446 and 3463 cm^{-1} for the α-phase and the β-phase of PyM3 and 3485 and 3491 cm^{-1} for the α-phase and the β-phase of PyT3, respectively. This indicates that in the β-phase PyM3 and PyT3 crystals, after the thermally induced irreversible phase transition, the molecules are arranged with weaker hydrogen bonding of the chiral OH groups compared to those of the α-phase crystals.

The β-phase PyM3 crystals exhibit a large SHG activity two times larger than that of DAT2 crystal, similar to the one observed in the α-phase crystal. Therefore, the crystal structures for the PyM3 are changed from one non-centrosymmetric arrangement to a different non-centrosymmetric arrangement. Particularly interesting is the transition in PyT3 crystals. The

ADVANCED FUNCTIONAL MATERIALS

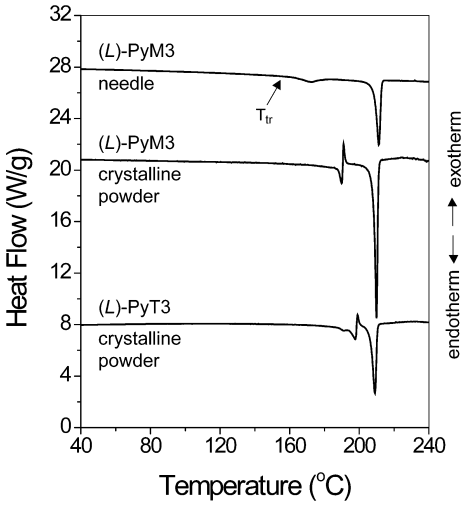

Figure 7. DSC thermograms of L-PyM3 and L-PyT3 crystals with different morphology (10 K min^{-1} scan rate).

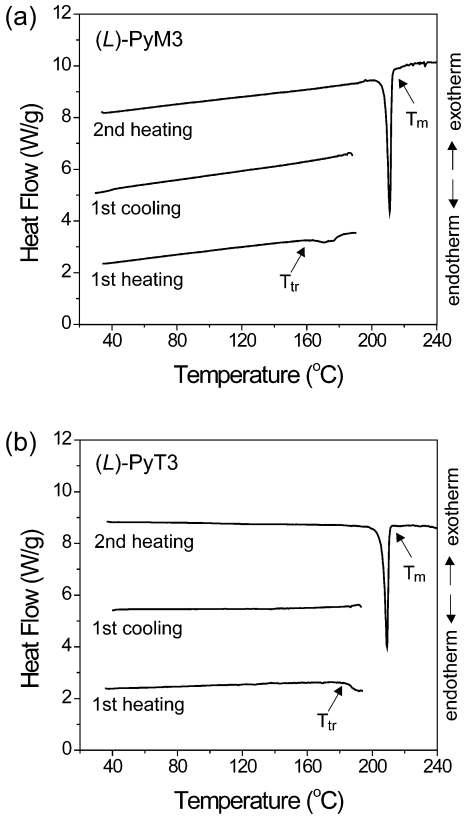

Figure 8. DSC thermograms showing the irreversible phase transitions of needlelike L-PyM3 and crystalline powder L-PyT3 crystals (10 K min^{-1} scan rate).

β-phase of the PyT3 crystals also exhibit a large SHG activity two orders of magnitude larger than that of urea, although the α-phase is inactive. This indicates that during the phase transition of PyT3 crystal, the centrosymmetric α-phase crystal is transformed into a non-centrosymmetric β-phase. To our knowledge this is the first observation of a phase transition from a centrosymmetric to a polar crystalline symmetry upon heating of an organic nonlinear optical crystal.

3. Conclusions

We have synthesized and characterized a series of new nonlinear optical crystals based on configurationally locked polyene (CLP) containing chiral hydroxyl pyrrolidine donors. All CLP derivatives exhibit a high thermal stability with decomposition temperatures T_d of at least 270 °C. Single crystals of the enantiopure D- and L-PyM3 with monoclinic space group $P2_1$ exhibit macroscopic nonlinearities two times larger than previously reported analogous DAT2 crystals with a similar molecular nonlinearity. This is due to favorable crystalline packing with strong hydrogen-bonded polar polymer-like chains of prolinol-based PyM3 molecules, which are very-well aligned along the polar crystallographic *b*-axis. Therefore, the acentric CLP crystals with large thermal stability are very attractive for melt-based crystal growth engineering for nonlinear optical applications. Additionally five CLP crystals grown from solution exhibit a thermally induced structural phase transition crystals from an α-phase to a β-phase. These phase transitions have been found to be reversible in PyT1 crystal and irreversible in D-PyM3, L-PyM3, D-PyT3, and L-PyT3 crystals. Compared to the α-phase, the β-phase of CLP crystals typically shows a lower symmetry with increased second-order nonlinear optical activity. To the best of our knowledge this is the first observation of such a behavior in organic nonlinear optical crystals with large molecular dipole moments.

4. Experimental

Synthesis: All chemicals were obtained from commercial suppliers (Aldrich) and used without further purification. To introduce the chirality of the hydroxyl group on the pyrrolidine ring of the chromophores, the enantiopure pyrrolidine derivatives such as D-3-pyrrolidinol (98 %), D-prolinol (99 %), and L-prolinol (99 %) were used. The chromophores were synthesized by two consecutive Knoevenagel condensations with the corresponding aldehydes according to the literature [15–17].

PyT1: ^{1}H NMR ($CDCl_3$, δ): 7.4 (d, J = 8.7 Hz, 2H, Ar-H), 7.0 (d, J = 15.9 Hz, 1H, –CH=CH–), 6.8 (d, J = 15.9 Hz, 1H, –CH=CH–), 6.7 (s, 1H, –C=CH–), 6.5 (d, J = 8.7 Hz, 2H, Ar-H), 3.4 (t, 4H, N–CH_2), 2.6 (s, 2H, –CH_2), 2.5 (s, 2H, –CH_2), 2.0 (t, 4H, –CH_2–), 1.0 (s, 6H, –CH_3). ^{13}C NMR ($CDCl_3$, δ): 169.01, 155.35, 148.96, 138.50, 129.57, 123.57, 122.92, 121.03, 114.34, 113.55, 111.94, 77.03, 47.68, 43.09, 39.35, 32.09, 28.19, 25.58. Anal. calcd for $C_{23}H_{25}N_3$ (343.47): C 80.43, H 7.34, N 12.23; Found C 80.59, H 7.32, N 12.21.

D-PyT2: ^{1}H NMR ($CDCl_3$, δ): 7.4 (d, J = 8.4 Hz, 2H, Ar-H), 7.0 (d, J = 15.3 Hz, 1H, –CH=CH–), 6.8 (d, J = 15.3 Hz, 1H, –CH=CH–), 6.7 (s, 1H, –C=CH–), 6.5 (d, J = 8.7 Hz, 2H, Ar-H), 4.7 (m, 1H, CH–OH), 3.6 (m, 2H, N–CH_2–O), 3.5–3.3 (m, 2H, N–CH_2), 2.6 (s, 2H, –CH_2), 2.5 (s, 2H, –CH_2), 2.1 (m, 2H, –CH_2–), 1.7 (d, 1H, –OH), 1.0 (s, 6H, –CH_3). ^{13}C NMR ($CDCl_3$, δ): 169.12, 155.24, 148.83, 138.26, 129.50, 123.97, 123.45, 121.22, 114.20, 113.48, 112.01, 76.91, 70.97, 56.01, 45.41, 42.90, 39.15, 34.03, 31.89, 27.96. Anal. calcd for $C_{23}H_{25}N_3O$ (359.47): C 76.85, H 7.01, N 11.69, O 4.45; Found C 76.62, H 7.07, N 11.67, O 4.65.

D-PyT3 and L-PyT3: ^{1}H NMR ($CDCl_3$, δ): 7.4 (d, J = 8.7 Hz, 2H, Ar-H), 7.0 (d, J = 15.9 Hz, 1H, –CH=CH–), 6.8 (d, J = 15.9 Hz, 1H,

–CH=CH–), 6.7 (s, 1H, –C=CH–) 6.5 (d, J = 8.7 Hz, 2H, Ar-H), 4.0 (m, 1H, N–CH), 3.7–3.6 (m, 2H, N–CH_2–O), 3.5 (m, 1H, N–CH_2), 3.3 (m, 1H, N–CH_2), 2.6 (s, 2H, –CH_2), 2.5 (s, 2H, –CH_2), 2.1 (m, 4H, –CH_2–), 1.0 (s, 6H, –CH_3). ^{13}C NMR ($CDCl_3$, δ): 169.08, 155.12, 148.96, 138.03, 129.47, 124.24, 123.81, 121.39, 114.20, 113.42, 112.60, 77.05, 63.33, 60.11, 49.10, 43.01, 39.34, 32.10, 28.64, 28.18, 23.58. Anal. calcd for $C_{24}H_{27}N_3O$ (373.50): C 77.18, H 7.29, N 11.25, O 4.28; Found C 76.94, H 7.30, N 11.19, O 4.49.

PyM1: ^{1}H NMR ($CDCl_3$, δ): 7.4 (d, J = 8.7 Hz, 2H, Ar-H), 7.0 (d, J = 15.6 Hz, 1H, –CH=CH–), 6.8 (d, J = 15.6 Hz, 1H, –CH=CH–), 6.7 (s, 1H, –C=CH–), 6.5 (d, J = 8.7 Hz, 2H, Ar-H), 3.4 (t, 4H, N–CH_2), 2.7 (t, 2H, –CH_2), 2.6 (t, 2H, –CH_2), 2.0 (m, 4H, –CH_2–), 1.9 (m, 2H, –CH_2). ^{13}C NMR ($CDCl_3$, δ): 169.62, 157.15, 149.00, 138.61, 129.58, 123.33, 122.89, 122.08, 114.25, 113.48, 111.88, 76.91, 47.50, 29.41, 25.35, 25.11, 21.29. Anal. calcd for $C_{21}H_{21}N_3$ (315.42): C 79.97, H 6.71, N 13.32; Found: C 79.78, H 6.74, N 13.24.

D-PyM2: ^{1}H NMR ($CDCl_3$, δ): 7.4 (d, J = 8.7 Hz, 2H, Ar-H), 7.0 (d, J = 15.6 Hz, 1H, –CH=CH–), 6.8 (d, J = 15.6 Hz, 1H, –CH=CH–), 6.7 (s, 1H, –C=CH–), 6.5 (d, J = 8.7 Hz, 2H, Ar-H), 4.7 (m, 1H, CH–OH), 3.6 (m, 2H, N–CH_2–O), 3.5–3.3 (m, 2H, N–CH_2), 2.7 (t, 2H, –CH_2), 2.6 (t, 2H, –CH_2), 2.0 (m, 2H, –CH_2–), 1.9 (m, 2H, –CH_2), 1.7 (d, 1H, –OH). ^{13}C NMR ($CDCl_3$, δ): 169.60, 156.99, 148.83, 138.39, 129.55, 123.76, 123.46, 122.32, 114.21, 113.45, 112.05, 77.05, 71.09, 56.18, 45.60, 34.24, 29.62, 25.33, 21.50. Anal. calcd for $C_{21}H_{21}N_3O$ (343.47): C 76.11, H 6.39, N 12.68, O 4.83; Found: C 75.85, H 6.45, N 12.55, O 5.05.

D-PyM3 and L-PyM3: ^{1}H NMR ($CDCl_3$, δ): 7.4 (d, J = 8.7 Hz, 2H, Ar-H), 7.0 (d, J = 15.9 Hz, 1H, –CH=CH–), 6.8 (d, J = 15.9 Hz, 1H, –CH=CH–), 6.7 (s, 1H, –C=CH–), 6.5 (d, J = 8.7 Hz, 2H, Ar-H), 4.0 (m, 1H, N–CH), 3.7–3.6 (m, 2H, N–CH_2–O), 3.5 (m, 1H, N–CH_2), 3.3 (m, 1H, N–CH_2), 2.7 (t, 2H, –CH_2), 2.6 (t, 2H, –CH_2), 2.0 (m, 4H, –CH_2<C)>, 1.9 (m, 2H, –CH_2). ^{13}C NMR ($CDCl_3$, δ): 169.59, 156.90, 148.98, 138.14, 129.50, 124.00, 123.77, 122.46, 114.16, 113.39, 112.57, 77.03, 63.34, 60.09, 49.10, 29.62, 28.65, 25.33, 23.58, 21.49. Anal. calcd for $C_{22}H_{23}N_3O$ (343.47): C 76.49, H 6.71, N 12.16, O 4.63; Found: C 76.22, H 6.89, N 12.06, O 4.82.

X-Ray Structure Analysis: Single-crystal X-ray diffraction experiments for various CLP crystals grown using the slow-evaporation method in solution were carried out on a single-crystal X-ray diffractometer equipped with a CCD detector (Xcalibur PX, Oxford Diffraction) with a 65 mm sample–detector distance. Data reduction and numerical absorption were performed using the software package CrysAlis [23]. The crystal structures were solved by direct methods and the full data sets refined on F^2, employing the programs SHELXS-97 and SHELXL-97 [24,25]. Crystallographic data (excluding structure factors) for the structures reported in this paper have been deposited with the Cambridge Crystallographic Data Center. Copies of the data can be obtained free of charge via www.ccdc.cam.ac.uk/conts/retrieving.html.

Red Plate-Like PyT1 Crystal (α Phase): $C_{23}H_{25}N_3$, M_r = 343.46, monoclinic, space group $P2_1$, a = 5.9510(12) Å, b = 7.5960(15) Å, c = 21.590(4) Å, α = 90°, β = 96.82(3)°, γ = 90°, V = 969.0(3) Å^3, T = 295 K, CCDC 293 252.

Needle-Like L-PyM3 crystal (α Phase): $C_{22}H_{23}N_3O$, M_r = 345.43, monoclinic, space group $P2_1$, a = 5.6260(11) Å, b = 14.622(3) Å, c = 11.601(2) Å, α = 90°, β = 99.67(3)°, γ = 90°, V = 940.8(3) Å^3, T = 295 K, CCDC 286 962.

Red Plate-Like DAT2 Crystal: $C_{21}H_{23}N_3$, M_r = 317.42, monoclinic, space group $P2_1$, a = 6.1303(7) Å, b = 7.4239(9) Å, c = 20.258(4) Å, α = 90°, β = 96.750(8)°, γ = 90°, V = 915.6(2) Å^3, T = 295 K, CCDC 278 087.

Received: June 7, 2006
Revised: September 12, 2006

[1] K. J. Vahala, *Nature* **2003**, *424*, 839.
[2] C. Bosshard, M. Bösch, I. Liakatas, M. Jäger, P. Günter, in *Nonlinear Optical Effects and Materials* (Ed: P. Günter), Springer, Berlin **2000**, Ch. 3.
[3] H. S. Nalwa, T. Watanabe, S. Miyata, in *Nonlinear Optics of Organic Molecules and Polymers* (Eds: H. S. Nalwa, S. Miyata), CRC Press, Boca Raton, FL **1997**, Ch. 4.
[4] M. G. Kuzyk, C. W. Dirk, in *Characterization Techniques and Tabulations for Organic Nonlinear Optical Materials*, Marcel Dekker, New York **1998**.
[5] L. R. Dalton, *J. Phys. Condens. Matter* **2003**, *15*, 897.
[6] M. He, T. M. Leslie, J. A. Sinicropi, S. M. Garner, L. D. Reed, *Chem. Mater.* **2002**, *14*, 4669.
[7] M. S. Wong, V. Gramlich, C. Bosshard, P. Günter, *J. Mater. Chem.* **1997**, *7*, 2021.
[8] F. Pan, M. S. Wong, V. Gramlich, C. Bosshard, P. Günter, *Chem. Commun.* **1996**, 1557.
[9] H. L. Bozec, T. L. Bouber, O. Maury, A. Bondon, I. Ledoux, S. Deveau, J. Zyss, *Adv. Mater.* **2001**, *13*, 1677.
[10] B. R. Cho, S. J. Lee, S. H. Lee, K. H. Son, Y. H. Kim, J. Y. Doo, G. J. Lee, T. I. Kang, Y. K. Lee, M. Cho, S. J. Jeon, *Chem. Mater.* **2001**, *13*, 1438.
[11] S. R. Marder, J. W. Perry, C. P. Yakymyshyn, *Chem. Mater.* **1994**, *6*, 1137.
[12] F. Pan, G. Knöpfle, C. Bosshard, S. Follonier, R. Spreiter, M. S. Wong, P. Günter, *Appl. Phys. Lett.* **1996**, *69*, 13.
[13] K. Staub, G. A. Levina, S. Barlow, T. C. Kowalczyk, H. S. Lackritz, M. Barzoukas, A. Fort, S. R. Marder, *J. Mater. Chem.* **2003**, *13*, 825.
[14] Y. C. Shu, Z. H. Gong, C. F. Shu, E. M. Breitung, R. J. McMahon, G. H. Lee, A. K.-Y. Jen, *Chem. Mater.* **1999**, *11*, 1628.
[15] S. Ermer, S. M. Lovejoy, D. S. Leung, H. Warren, C. R. Moylan, R. J. Twieg, *Chem. Mater.* **1997**, *9*, 1437.
[16] O. P. Kwon, B. Ruiz, A. Choubey, L. Mutter, A. Schneider, M. Jazbinsek, P. Günter, *Chem. Mater.* **2006**, *18*, 4049.
[17] O. P. Kwon, J. H. Im, J. H. Kim, S. H. Lee, *Macromolecules* **2000**, *33*, 9310.
[18] S. K. Kurtz, T. T. Perry, *J. Appl. Phys.* **1968**, *39*, 3798.
[19] a) I. Weissbuch, M. Lahav, L. Leiserowitz, *Cryst. Growth Des.* **2003**, *3*, 125. b) I. Weissbuch, R. Popovivitz-Biro, M. Lahav, L. Leiserowitz, *Acta Crystallogr., Sect B: Struct. Sci.* **1995**, *51*, 115.
[20] J. Zyss, J. F. Nicoud, M. Coquillay, *J. Chem. Phys.* **1984**, *81*, 4160.
[21] D. Giron, *Thermochim. Acta* **1995**, *248*, 1.
[22] K. Sato, *J. Phys. D* **1993**, *26*, B77.
[23] http://www.oxford-diffraction.com.
[24] G. Sheldrick, SHELXS-97. Program for the Solution of Crystal Structures, University of Göttingen, Germany **1997**.
[25] G. Sheldrick, SHELXL-97. Program for the Refinement of Crystal Structures, University of Göttingen, Germany **1997**.